Eur. Phys. J. A **3**, 281–292 (1998)

THE EUROPEAN PHYSICAL JOURNAL A

Fast fission mechanism and duality of the diffusion process

H. Baba, N. Takahashi, A. Yokoyama[a], T. Saito

Department of Chemistry, Graduate School of Science, Osaka University, 1-1 Machikaneyama, Toyonaka, Osaka 560, Japan

Received: 11 November 1997
Communicated by P. Armbruster

Abstract. The reaction of ^{238}U with ^{12}C was studied radiochemically with the purpose of elucidating fast fission characteristics. From the difference in the mass distribution below and above the critical energy where fast fission is predicted to set in, fast fission component was extracted in far-asymmetric mass region and interpreted as the mass diffusion following the Fokker-Planck equation. Anomalous charge dispersion widths in the corresponding mass region and a sudden increase of the whole mass distribution width at the critical energy were also observed to support the above result. The reaction time of fast fission deduced from the width and position of the mass distribution was 5×10^{-21}s as well by taking into account the effect of neutron emission during the diffusion process, which turned out to be more than one order of magnitude longer than the corresponding life time of typical deep inelastic scattering but substantially short compared to ordinary fusion-fission life time. Evaluation of the driving potential for mass drift required dinuclear configuration be of an elongated or deformed form for fast fission in contrast to a more compact form for the deep-inelastic process.

PACS. 25.70.Jj Fusion and fusion-fission reactions – 25.85.Ge Charged-particle-induced fission

1 Introduction

The effect of the angular momentum on the fission phenomenon appears as decrease of the fission barrier [1-4]. The fission barrier finally vanishes when the angular momentum introduced to the compound nucleus exceeds a critical value ℓ_{B_f}. The fission with no fission barrier is called fast fission. Though the definition of fast fission is thus quite clear, the mechanism of formation of the system undertaking fast fission is not quite distinguished from deep inelastic scattering, quasi-fission, etc. The characteristics of fast fission are not very well known either in spite of several experimental and theoretical works [5-17].

Grègoire *et al.* [6,8,9] have concluded that fast fission is an intermediate mechanism between compound nucleus formation and deep inelastic collision by means of a dynamical approach [11] for dissipative heavy-ion collisions leading either to a compound nucleus or to fast fission. Subsequently, they claim fast fission is a long-lived deep inelastic component [7]; that is, fast fission lasts very long ($\sim 10^{-20}$ s) so that the angular distribution has $1/\sin\theta$ dependence and the mass asymmetry has been almost completely relaxed to give a symmetric mass distribution. Furthermore, the total kinetic energy of the products is expected to be the same for fast fission and for compound fission. According to them, the characteristics are observed only as broadening of the product mass distribution [6-11,13].

Heusch *et al.* [14] observed the angular distribution of products, Z distribution of the angle-integrated cross section and the mass distribution width for the 490-MeV ^{84}Kr plus ^{27}Al reaction to extract a fully damped reaction component distinguished from deep-inelastic products by a $1/\sin\theta$ angular distribution and from compound fission by a different Z distribution due to an incomplete mass asymmetry relaxation. Hefter treated theoretically fast fission as a dissipative collision leading to fusion immediately followed by fission by the "inverse mean-field" method [10].

Zheng *et al.* [12] also found that the difference in the total kinetic energy was too small to detect between fusion fission and fast fission. On the other hand, they observed substantial increase both in the widths of mass and kinetic energy distributions for fast fission. Gippner *et al.* [17] treated collisions of ^{32}S (192 MeV) + ^{238}U and ^{40}Ar (220 MeV) + ^{232}Th with one-dimensional diffusion model based on a calculated driving potential to deduce the existence of two independent modes of the mass relaxation process, the "fast-fusion" channel leading to a symmetric mass distribution and the "quasifission" process driving to an asymmetric mass distribution due to incomplete mass relaxation.

To summarize the above-mentioned discussions, fast fission is understood either as the statistical fluctuation controlled by the stiffness coefficient and the temperature

[a] To whom correspondence should be addressed.
tel.: +81-6-850-5417, fax.: +81-6-850-5418
(e-mail:yokoyama@chem.sci.osaka-u.ac.jp)

of the trapped system or as the mass relaxation due to diffusion process. No matter which mechanism is controlling fast fission, experiments tell us it is difficult to distinguish fast fission from normal fusion fission in terms of the product angular distribution, total kinetic energy or the mass asymmetric degree of freedom. Instead, widths of the mass and kinetic energy distributions are reported to be substantially large for fast fission compared to those of compound fission. The product charge distribution is also shown to be different between the two mechanisms.

The above consequences suggest the fast fission characteristics may be prominently observable in the form of broadening of the distribution width of various fission observables. On the other hand, it has been shown that counter experiments hardly succeeded in distinguishing fast fission phenomena from those of ordinary fusion fission. This is probably a consequence of smearing out of any fine structure in the distribution of fission observables due to finite mass and/or energy resolution.

The conventional radiochemical technique which is able to strictly specify A and Z of the product nuclei is expected to supply sufficient information to isolate fast fission from ordinary fusion fission and subsequently to shed light on the mechanism of fast fission.

The present purpose is thus to radiochemically investigate the characteristics of the ^{12}C-induced fission of ^{238}U at incident energies below and above the borderline for the appearance of fast fission. Any notable difference in the feature between them, if any, should demonstrate the fast fission characteristics.

2 Experimental

^{238}U targets were prepared by electrodeposition of UO_2 on Al backing foils. Details of the procedure are described elsewhere [18]. The target assembly consisting of thus prepared ^{238}U target of about 1 mg/cm^2 in thickness and Al catcher foils to retain all fission product nuclei was irradiated with ^{12}C beams in a pneumatic irradiation facility installed in the AVF cyclotron at Research Center for Nuclear Physics, Osaka University.

^{238}U was irradiated with 110-, 130-, and 140-MeV ^{12}C for three hours and the irradiated target was subjected to off-line Ge γ-ray spectrometry. 30-min irradiation was undertaken as well in order to determine the yields of short-lived activities. Further, iodine and rare earths were chemically separated as described elsewhere [19] in separate runs before Ge γ-ray measurement. Chemical yields were determined by comparing the yields of common nuclides between the destructive and non-destructive samples.

Obtained series of time-sequential γ-ray spectra were analyzed by BOB code [20] to construct decay curves for individual yields of the relevant photopeaks at the end of bombardment (EOB). The energy and the half-life of the relevant γ ray let us allow to identify the nuclide to which the γ ray belongs, and the obtained EOB value, corrected for the ingrowth during irradiation [21], is converted to the formation cross section. Gamma-ray emission probabilities and half-lives used to deduce cross section values were taken from the table by Reus and Westmeier [22].

3 Results

Resulting independent and fractional cumulative yields are summarized in Table 1 for three incident energies. Three or more isobaric yield data sets were obtained for several mass chains, from which we constructed charge dispersion curves by the least squares fit to the Gaussian distribution. Resulting charge dispersions are depicted in Fig. 1 for 140 MeV carbons. Furthermore, determined dispersion widths are plotted versus fragment mass A in Fig. 2. From Fig. 2, we can draw the following conclusions; i) the width is independent of A except for the far-asymmetric mass division in the case of the 140-MeV incident energy and the constant width agreed with dispersion widths observed among various types of energetic fissions within the experimental error [19], ii) the charge dispersion in the mass chains A=132 and 134 reveal complex features indicating coexistence of complete and incomplete fusion fission as mentioned by Lee *et al.* [23], and iii) the widths at far-asymmetric mass region were definitely large for 140-MeV beam compared to the normal value.

The broadening of charge dispersion width in far-asymmetric mass region is expected to represent the effect of fast fission since it sets in above 110 MeV. That is, the products of fast fission may locate in the far asymmetric mass region only.

Results of the fission fragment angular correlation measurement [19] tell us the incomplete fusion fission takes place by fusion of ^{4}He with the incident velocity produced due to break-up of the ^{12}C projectiles. With this knowledge, we determined apparent most probable charges $Z_{\rm p}$ for mass chains in which two or more isobaric yields were given. The obtained $Z_{\rm p}$ values are listed in Table 2 and visualized in Fig. 3. The $Z_{\rm p}$ values are found to clearly follow a linear relationship (solid lines) with A in all the cases except for the double-magic mass region. In the top of Fig. 3, the regions where incomplete fusion fission and sequential fission give substantial influence are indicated with horizontal segments of line for the ^{238}U fission with 240-MeV carbon beam [23].

The charge distribution in the light-ion-induced fission can be systematically treated [24-26] as

$$Z_{\rm p} = \frac{Z_{\rm c}}{A_{\rm c} - \nu_{\rm pre}}\{A + \nu_{\rm post}(A) \pm \Delta(A)\}, \qquad (1)$$

where $A_{\rm c}$ and $Z_{\rm c}$ are the mass and charge of the compound nucleus, $\nu_{\rm pre}$ and $\nu_{\rm post}$ give the numbers of pre- and post-scission neutrons, and Δ is the charge polarization. Here, $\nu_{\rm pre}$ is found to linearly depend on the excitation energy $E_{\rm x}$;

$$\nu_{\rm pre} = \frac{E_{\rm x}}{\alpha} + \nu_0. \qquad (2)$$

Then, we assumed the following values; α = 7.5 MeV, ν_0 = 18.5$-$ $Z_{\rm c}^2/(2A_{\rm c})$, $\nu_{\rm post}$ = 2.7, and Δ = 1.7 within the

Table 1. Independent (σ_I) and cumulative (σ_C) yields of the ^{238}U fission with ^{12}C of three incident energies

Nuclide	Half-life	110 MeV		130 MeV		140 MeV	
		σ_I(mb)	σ_C(mb)	σ_I (mb)	σ_C(mb)	σ_I(mb)	σ_C(mb)
^{71}Zn^{m}	3.94 h			-	1.37±0.17	-	1.23±0.09
^{72}Zn	46.5h	0.43±0.05	0.915±0.042	0.68±0.08	1.29±0.08	0.92±0.05	1.68±0.05
^{72}Ga	14.10h			1.0±0.8	2.3±0.8	1.6±0.7	3.8±0.8
^{73}Ga	4.86h	0.34±0.32	1.18±0.32			2.1±0.5	3.37±0.47
^{77}Ge$^{g(+m)}$	11.3 h	0.92±0.15	1.92±0.15	1.30±0.20	2.41±0.20	1.6±0.8	2.8±0.8
^{78}Ge	1.47h	1.33±0.26	2.26±0.26	1.52±0.16	2.34±0.16	1.23±0.18	1.86±0.18
^{78}As	1.51h			0.54±0.90	2.9±0.9		
^{82}Br^{g+m}	35.3h	1.54±0.12	-	2.21±0.16	-	3.07±0.17	-
^{82}Rb^{m}	6.47h					0.44±0.44	
^{83}Se^{g}	22.5m			-	4.4±1.3		
^{84}Br^{g}	31.8m			-	4.9±1.8	-	2.25±0.30
^{84}Rb^{g+m}	32.87d				0.51±0.07		
^{85}Kr^{m}	4.48h		4.25±0.26	-	5.20±0.32	-	8.1±0.5
^{87}Kr	76.3m	3.2±0.9	6.4±0.9	4.7±0.7	8.4±0.7	3.6±0.5	6.17±0.45
^{88}Kr	2.84h	3.1±0.6	5.2±0.6	4.3±0.9	6.5±0.9	4.8±1.7	7.0±1.7
^{88}Rb	17.8m					3.3±2.3	10.3±2.3
^{88}Y	106.6d						0.50±0.05
^{89}Rb	15.4m			4.1±1.2	9.7±1.2	5.4±0.6	11.6±0.6
^{90}Y^{m}	3.19h	0.76±0.06	-	1.53±0.11	-	2.06±0.20	-
^{91}Sr	4.52h	4.5±0.6	12.1±0.6	7.4±0.7	16.2±0.7	9.3±0.7	19.5±0.7
^{91}Y^{m}	49.71m	0.88±0.21	-	3.15±0.25		5.8±0.7	-
^{92}Sr	2.71h	5.4±0.6	10.8±0.6	8.1±1.2	14.2±1.2	10.3±2.3	17.5±2.3
^{92}Y	3.54h	-	14.6±1.1	11.4±1.3	24.8±1.4	11.1±1.5	28.6±2.5
^{92}Nb^{m}	10.15d					0.104±0.016	
^{93}Y	10.1h	5.3±1.6	14.9±1.2	8.9±2.5	22.4±2.5	9.9±2.6	23.8±2.6
^{94}Y	18.6m	7.1±3.2	16.2±3.2	10.1±1.5	19.5±1.5	10.0±1.2	18.5±1.2
^{95}Y	10.3m			12.5±0.6	19.5±0.6		
^{95}Zr	64.03d	5.0±1.2	19.3±1.2	9.7±0.9	28.4±0.9	10.1±2.7	27.5±2.7
^{95}Nb^{g+m}	34.98d	1.38±0.48	20.8±1.3	4.0±2.4	32.4±2.5	3.46±0.26	31.0±2.8
^{96}Nb	23.35h	2.54±0.18	-	5.69±0.32	-	6.39±0.17	-
^{97}Zr	17.0h	9.0±1.3	18.4±1.3	13.2±1.4	22.8±1.4	13.1±0.6	21.5±0.6
^{98}Nb^{B}	51.3m	12.9±0.7	-	11.5±1.5	-	12.1±0.9	-
^{99}Mo	2.75d	4.2±1.6	24.9±1.6	9.3±1.2	38.7±1.2	9.5±1.2	39.4±1.2
^{99}Tc^{m}	6.01h	-	24.8±1.6	0.21±0.37	38.9±1.3	0.52±0.07	39.4±1.5
^{101}Mo	14.6m			18.5±2.8	39.8±2.8		
^{101}Tc	14.2m					-	46.8±2.2
^{101}Rh^{m}	4.34d					-	0.57±0.10
^{103}Ru	39.25d	3.1±1.6	31.0±1.6	6.2±2.2	44.0±2.2	7.7±4.4	48.4±4.2
^{104}Tc	18.4m			16.4±1.5	31.1±1.5	17.6±2.0	31.7±2.0
^{105}Ru	4.44h	7.1±1.0	30.0±1.0	12.6±1.5	41.5±1.5	23.7±1.7	42.3±1.7
^{105}Rh^{g+m}	35.36h		29.1±1.6	4.4±1.4	40.8±1.7	3.2±4.0	46.1±3.5
^{106}Ru	371.6d	11.2±3.4	28.7±3.4	17.7±4.1	36.8±4.1	15±6	29.5±5.5
^{107}Rh	21.7m	5.4±3.9	24.6±3.9	6.9±2.7	35.6±2.7	8±7	34.8±6.9
^{110}Ag^{m}	249.9d	2.04±0.30	-	2.5±0.6	-	4.28±0.34	-
^{111}Pd^{m}	5.5h	8.8±0.5	-	11.3±1.5	-	12.5±0.6	-
^{111}Ag^{g+m}	7.45d	3.6±3.4	31.9±3.4	9.4±7.1	48.3±4.5	9.6±5.2	43.5±5.2
^{111}In^{g+m}	2.83d			-	0.276±0.029	-	0.33±0.13
^{112}Pd	21.05h	14.7±1.9	28.2±1.9	19.5±2.0	31.9±2.0	21.9±3.0	34.3±3.0
^{112}Ag	3.14h	10.3±1.7	38.5±2.8	9.2±1.2	41.1±2.3	12.4±0.7	48.4±2.2
^{113}Ag^{g}	5.37h	-	34.8±3.2	-	54.6±3.1		
^{115}Ag^{g}	20.0m			-	16.0±0.9		
^{115}Cd^{g}	2.23d	-	23.1±0.9	-	27.8±1.1	-	26.7±2.1
^{115}In^{m}	4.49h	-	23.2±0.9				
^{117}Cd^{g}	2.94h	-	24.6±0.9	-	24.0±1.1	-	24.1±2.0
^{117}Cd^{m}	3.36h	17.9±0.8		17.0±0.7		17.1±3.4	
^{117}In^{g}	43.8m			5.5±0.7	35.7±1.9	6.91±0.24	35.7±3.4
^{117}In^{m}	1.94h	2.84±0.22	-	5.5±1.1		4.0±0.5	

Table 1. Continued.

Nuclide	Half-life	110 MeV		130 MeV		140 MeV	
		σ_I(mb)	σ_C(mb)	σ_I (mb)	σ_C(mb)	σ_I(mb)	σ_C(mb)
$^{117}Sn^{m}$	13.61d	1.03±0.07	-	3.62±0.31	-	4.2±0.8	-
$^{118}Sb^{m}$	5.00h			1.22±0.07	-	0.96±0.38	-
^{118}Te	6.00d					-	0.14±0.05
$^{119}Te^{m}$	4.69d					0.60±0.08	-
$^{120}Sb^{B}$	5.76d	1.38±0.09	-	3.57±0.28	-	4.78±0.20	-
$^{121}Te^{g}$	16.8d			0.224±0.029	1.88±0.27	1.18±0.08	2.68±0.12
$^{121}Te^{m}$	154d			1.37±0.55		1.37±0.09	
^{121}I	2.12h					0.17±0.08	-
$^{122}Sb^{g+m}$	2.70d	8.15±0.41	-	14.4±0.8	-	16.2±1.4	-
$^{123}Sn^{m}$	40.08m			-	6.1±0.8	-	5.5±0.8
$^{123}Te^{m}$	119.7d	2.15±0.18	-	7.06±0.45	-	7.5±0.9	-
^{123}I	13.2h			1.12±0.11	1.22±0.11	1.26±0.13	1.38±0.13
$^{124}Sb^{g+m}$	60.2d	14.9±0.7	-	18.8±1.7	-	21.4±1.1	-
^{124}I	4.18d			1.60±0.25	-	3.8±0.8	-
$^{125}Sn^{g}$	9.64d	-	6.4±0.7	-	5.9±0.7	-	5.1±0.7
^{125}Sb	2.73y	13.8±2.2	23.9±2.2			7.6±2.3	24.9±5.4
$^{126}Sb^{g}$	12.40d	10.02±0.29	-	11.11±0.25	-	11.5±0.6	-
$^{126}Sb^{m}$	19.0m			3.4±0.8	-	2.3±0.6	-
^{126}I	13.02d	4.24±0.39	-	8.92±0.41	-	11.2±0.4	-
$^{127}Sn^{g}$	2.10h	-	8.1±1.1	-	7.6±1.8	-	6.6±3.6
^{127}Sb	3.85d	7.2±0.5	9.56±0.41	9.3±0.5	11.2±0.5	10.0±0.7	11.8±0.7
$^{127}Xe^{g+m}$	36.41d	2.70±0.35	-	2.13±0.10	-	3.63±0.45	-
$^{128}Sn^{g+m}$	59.1m	0.95±0.16	0.99±0.16	0.98±0.10	1.11±0.10	1.66±0.13	1.74±0.13
$^{128}Sb^{g}$	9.01h	-	3.10±0.15	-	5.67±0.29	-	4.09±0.39
^{128}I	25m			16.3±0.6	-	13.4±1.7	-
^{129}Sb	4.32h	2.53±0.22	2.88±0.22	3.1±0.6	3.4±0.6	1.8±0.5	1.88±0.42
$^{129}Te^{m}$	33.6d	-	14.8±1.5			-	13.6±1.5
^{129}Cs	32.1h			2.6±0.4	2.71±0.36		
$^{130}Sb^{A}$	40m			-	2.39±0.37	-	3.95±0.34
$^{130}I^{g+m}$	12.36h	13.00±0.34	-	14.0±0.7	-	14.9±1.0	
^{131}Sb	23.0m			-	4.0±1.6	-	3.86±0.39
$^{131}Te^{g}$	25m			2.63±0.55	10.8±1.0	2.7±1.3	12.1±1.5
$^{131}Te^{m}$	30h	3.47±0.26	-	4.60±0.44		5.22±0.37	
^{131}I	8.02d	-	17.0±0.8	-	19.4±0.9	-	19.7±1.2
$^{131}Ba^{g+m}$	11.8d			1.00±0.19	1.10±0.19	1.39±0.38	1.55±0.38
^{132}Te	3.26d	3.83±0.33	4.73±0.33	4.1±0.3	5.62±0.23	4.4±0.6	5.55±0.41
$^{132}I^{g+m}$	2.30h	8.1±0.6	12.8±0.7	7.6±0.8	13.2±0.8	10.5±2.1	16.3±2.2
^{132}Cs	6.48d	6.0±5.7	-	12.1±0.7	-	13.6±0.9	-
$^{133}Te^{m}$	55.4m	2.6±0.7	-	2.7±0.6	-	2.93±0.48	
$^{133}I^{g+m}$	20.8h	-	8.8±0.5	-	11.9±0.8	-	12.1±0.5
$^{133}Xe^{g+m}$	5.29d	10.2±0.7	18.9±0.9	13.3±1.3	24.6±1.5	7.6±4.2	21.0±1.5
$^{133}Ba^{m}$	38.9h			5.5±0.6	-	9.8±1.9	
^{134}Te	41.8m	-	1.8±0.7	-	6.2±1.3	-	8.8±0.9
$^{134}I^{g+m}$	52.6m	6.3±0.7	8.1±0.6	11.4±0.6	17.6±1.2	8.9±1.4	17.7±1.6
$^{134}Cs^{g+m}$	2.06y	13.2±0.9	-	15.6±1.1	-	17.1±2.0	-
$^{134}Cs^{m}$	2.91h	10.8±1.2	-	11.4±1.2	-	15.2±1.2	-
^{135}I	6.61h	4.2±0.5	5.18±0.36	4.5±0.5	5.27±0.40	4.4±0.5	5.43±0.46
$^{135}Xe^{g}$	9.08h	5.41±0.35	10.6±0.5	5.0±0.5	11.8±0.6	3.1±1.1	11.9±1.2
$^{135}Xe^{m}$	15.6m			4.0±0.5		4.38±0.17	
$^{135}Cs^{m}$	53m			9.7±1.5	-	5.12±0.49	-
$^{135}Ba^{m}$	28.7h	-	6.5±0.6				
^{136}Cs	13.16d	8.94±0.41	-	9.24±0.27	-	9.64±0.20	-
$^{137}Ce^{m}$	34.4h			1.59±0.49	-		
$^{138}Cs^{g+m}$	32.2m	5.4±0.7	6.5±0.7	6.6±1.3	7.6±1.3	8.8±1.6	9.8±1.6
$^{138}Pr^{m}$	2.10h			0.204±0.038	-	2.28±0.30	-
^{139}Ba	1.38h	5.7± 0.8	9.0±0.8	10.6±1.4	13.0±1.4	11.2±0.7	13.6±0.7
$^{139}Ce^{g+m}$	137.7d	2.77±0.19	3.46±0.19	2.7±0.7	9.3±0.7	3.9±1.6	10.9±1.6

Table 1. Continued.

Nuclide	Half-life	110 MeV		130 MeV		140 MeV	
		σ_I(mb)	σ_C(mb)	σ_I (mb)	σ_C(mb)	σ_I(mb)	σ_C(mb)
$^{139}Nd^{m}$	5.5h			0.67±0.11	-		
^{140}Ba	12.75d	6.15±0.20	7.59±0.20	7.7±0.7	9.0±0.7	8.61±0.27	9.78±0.27
^{140}La	40.28h	7.68±0.38	15.26±0.43	9.79±0.26	18.8±0.6	9.62±0.45	19.1±0.7
^{141}Ba	18.27m						8.0±0.6
^{141}La	3.92h	5.7±1.7	9.4±1.7	9.5±1.4	12.3±1.4	9.4±2.0	12.9±1.5
^{141}Ce	32.50d	9.5±2.0	18.9±1.0	12.4±1.0	24.9±1.0	10.6±1.8	23.6±1.0
^{142}La	1.52h	5.9±0.5	6.81±0.43	7.0±0.5	7.40±0.46	7.7±0.7	8.1±0.5
$^{142}Pr^{g+m}$	19.13h			6.8±0.8	-	7.5±1.0	-
^{143}Ce	33.0h	7.8±0.9	12.9±0.9	10.5±0.8	13.8±0.8	10.5±0.6	13.7±0.6
^{144}Ce	284.9d	6.5±0.7	8.7±0.7	7.5±0.7	9.2±0.7	8.2±1.8	9.8±1.1
^{146}Pr	24.1m					6.6±4.7	8.1±4.7
^{146}Pm	5.53y			2.56±0.48	-		
^{147}Pr	13.6m			-	7.3±4.1	6.1±2.0	7.1±2.0
^{147}Nd	10.98d	7.2±0.2	12.8±0.8	9.1±0.5	13.85±0.44	9.1±0.8	13.0±0.8
^{147}Eu	24.0d			0.311±0.031	0.322±0.031		
$^{148}Pm^{g}$	5.37d	0.32±0.08	-	0.081±0.033	-	2.03±0.11	-
$^{148}Pm^{m}$	41.3d	3.09±0.31	-	5.18±0.16	-	8.0±0.7	-
^{149}Nd	1.73h	4.6±0.5	6.21±0.47	3.5±0.5	4.31±0.42	4.1±0.9	4.7±0.9
^{149}Pm	2.21d	6.5±1.9	12.7±1.8	8.0±1.5	12.1±1.4	9.6±2.9	14.4±2.9
^{149}Gd	9.4d	-	0.053±0.035	-	0.141±0.043		
^{150}Pm	2.68h	4.67±0.31	-	5.25±0.27	-	4.46±0.39	-
$^{150}Eu^{A}$	12.6h			0.77±0.18	-		
^{151}Pm	28.4h	4.7±0.4	6.66±0.40	5.3±0.5	6.61±0.43	4.8±0.5	5.94±0.49
$^{152}Eu^{m1}$	9.32h			0.96±0.24	-	0.99±0.24	-
$^{152}Eu^{m2}$	1.60h			0.195±0.025	-	0.94±0.38	-
$^{152}Tb^{g+m}$	17.5h			0.065±0.024	-		
^{153}Sm	46.7h	4.2±0.5	6.41±0.42	5.7±0.6	7.5±0.6	6.8±0.8	8.7±0.8
^{153}Tb	2.34d						1.03±0.09
$^{154}Tb^{g}$	21.4h			0.92±0.16	-		
$^{154}Tb^{m1}$	9.0h			0.152±0.028	-	0.249±0.035	
$^{154}Tb^{m2}$	22.6h	1.17±0.09	-	1.34±0.20	-	1.29±0.24	
^{155}Sm	22.1m			1.39±0.25	1.56±0.25	1.20±0.15	1.35±0.15
^{155}Eu	4.68y	5.8±2.8	7.9±2.8				
^{155}Tb	5.32d	0.71±0.28	0.75±0.28			2.44±0.28	3.15±0.28
^{156}Sm	9.4h	1.01±0.11	1.17±0.11			0.93±0.17	1.01±0.17
^{156}Eu	15.2d	2.50±0.25	3.62±0.22	2.76±0.35	3.38±0.35	2.56±0.21	3.13±0.21
$^{156}Tb^{g}$	5.35d	0.321±0.035	-			3.2±0.6	
$^{156}Tb^{m1}$	24.4h	0.96±0.10	-				
^{157}Eu	15.1h	2.44±0.20	2.69±0.20				
^{159}Gd	18.56h			1.74±0.16	2.11±0.16	1.78±0.21	1.98±0.21
^{160}Tb	72.3d	1.47±0.12	-	2.13±0.12	-	2.15±0.22	-
^{160}Er	28.6h						0.60±0.06
^{166}Tm	7.70h			0.50±0.21	0.63±0.22	0.85±0.09	1.30±0.14
^{166}Yb	2.36d		1.47±0.48				
^{167}Ho	3.1h	0.30±0.07	0.37±0.07				
^{167}Tm	9.24d	0.25±0.03	0.335±0.024	0.80±0.29	1.25±0.29	0.76±0.12	1.23±0.12
^{168}Tm	93.1d	0.48±0.14	-	0.65±0.06	-	0.96±0.11	-
$^{169}Yb^{g+m}$	32.02d					0.41±0.16	0.97±0.16
^{172}Er	2.05d						0.031±0.015
$^{172}Lu^{g+m}$	6.70d			0.139±0.013	-	0.167±0.015	-
^{175}Hf	70.0d	0.12±0.11	0.17±0.11			0.26±0.18	0.49±0.18
^{225}Ac	10.0d						100±11
^{237}U	6.75d		70.5±3.8				
^{239}Np	2.36d		14.7±0.8				8.9±1.8
^{240}Np	65m		$(1.31\pm0.14)\times10^{3}$				

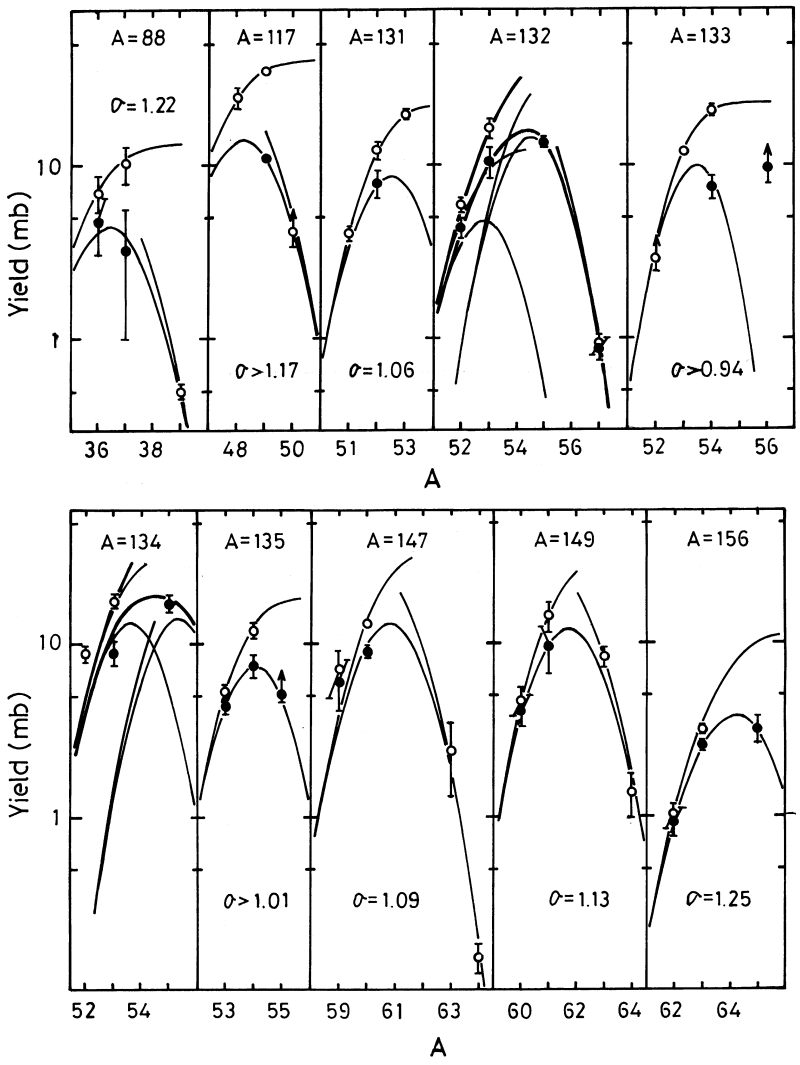

Fig. 1. Charge dispersion curves obtained for the 140-MeV incident energy. Closed circles indicate independent yields while open circles are for the partial cumulative yields. In the mass chain of 132 and 134, the charge dispersion of incomplete fusion fission is superimposed on the dispersion of fusion fission

allowance range [24-26] for respective quantities. The resulting charge distribution of the incomplete fusion fission is indicated in Fig. 3 with dashed lines for each incident energy. One may recognize that the most probable charges in the light-fragment mass region of the incomplete fusion fission coincide with those of the complete fusion fission for all three cases. This makes the evaluation of the total chain yields quite easy in this region.

The mass-yield distribution for 110-MeV ^{12}C is shown in Fig. 4 in which complete fusion fission (A), incomplete fusion fission (B), and the so-called "sequential fission (C)" are extracted. Solid marks represent the sum of the total chain yields of complete and incomplete fusion fissions evaluated by applying two different charge distributions. The complete fusion fission distribution was determined by fitting the outskirts of the whole mass distribution to a pair of the identical Gaussian curves (chain lines) [19]. The surplus portions were then attributed to incomplete-fusion and sequential fissions.

Figure 5 represents the mass distribution for the 130-MeV ^{12}C beam deduced by alike procedure as in the case of Fig. 4. The gross distribution (thick full line) was decomposed into three components, complete-fusion fission plus fast fission (trapezoidal thin full line), incomplete-fusion fission (B), and sequential fission (C).

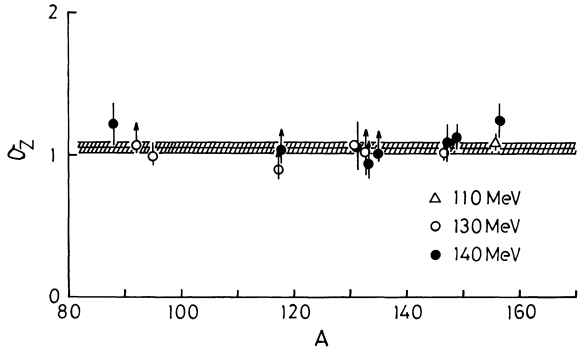

Fig. 2. Obtained width parameters plotted versus mass number A. The horizontal line with hatched band gives the weighted mean of the resulting widths except for the two outermost values at 140 MeV, namely, $< \sigma > = 1.05 \pm 0.04$ charge unit

Table 2. Apparent most probable charges determined with the sets of two or more isobaric yields using the charge dispersion curve with $\sigma = 1.05$ charge unit

A	110MeV	130MeV	140MeV	240MeV[a)]
72		30.25±0.85	$30.70^{+0.45}_{-0.55}$	31.35±0.25
78		31.75±1.35		$33.35^{+0.50}_{-1.00}$
82			<34.40+0.50	
84		<35.03−0.25		
87				36.75±0.10
88			36.75±0.10	36.90±0.10
91	>37.40−0.10	>37.60−0.05	>37.90−0.10	
92	$38.05^{+0.30}_{-0.45}$	38.65±0.05	$38.60^{+0.15}_{-0.30}$	
95	$39.05^{+0.20}_{-0.25}$	39.23±0.08	39.25±0.10	
96			40.30±0.30	$41.00^{+0.45}_{-0.30}$
97	40.55±0.10	40.00±0.05	40.00±0.05	$41.05^{+0.10}_{-0.15}$
99		41.30±0.05		
101			>42.20−0.10	
105		43.40±0.10	≤43.15+0.45	$44.40^{+0.45}_{-0.50}$
106		>43.75-0.50	>43.73-0.15	
111	$45.35^{+0.60}_{-0.45}$	45.90±0.10	46.10±0.20	≤46.55+0.05
112	$46.05^{+0.15}_{-0.20}$	45.92±0.20	46.00±0.15	46.43±0.15
117	>47.70−0.10	48.30±0.05	48.17±0.11	≥49.00−0.15
118			>48.45−0.35	
123		<50.90+0.10	<50.55+0.75	
124		$50.65^{+0.15}_{-0.10}$	51.05±0.15	
125			<52.00+0.55	
126	<51.50+0.15	51.75±0.05	51.90±0.05	≤52.65+0.10
127	52.10±0.10	51.95±0.05	52.18±0.10	52.53±0.10
128	>51.50−0.25	52.50±0.05	52.30±0.10	$53.10^{+0.25}_{-0.15}$
129		52.95±0.05	>53.50−0.40	53.25±0.10
130		<53.10+0.10	<52.83+0.15	
131	<53.90+0.20	52.73±0.06	52.46±0.11	$54.15^{+0.15}_{-0.10}$
132	53.62±0.12	53.00±0.10	53.38±0.35	$54.60^{+0.10}_{-0.05}$
		54.10±0.10	54.50±0.10	
133	$53.95^{+0.15}_{-0.20}$	53.87±0.10	53.48±0.11	
134	54.00±0.10	53.40±0.20	52.85±0.25	$52.95^{+0.55}_{-0.45}$
		53.90±0.10	53.90±0.10	
135	$53.85^{+0.25}_{-0.20}$	54.00±0.10	54.03±0.06	
138		>56.10−0.15	>56.65−0.10	56.40±0.10
139	$56.65^{+0.05}_{-0.10}$	57.00±0.10	57.05±0.10	56.40±0.10
140	56.40±0.05	56.80±0.10	56.75±0.05	56.50±0.15
141	57.95±0.20	57.90±0.25	57.67±0.25	$58.75^{+0.50}_{-0.40}$
142		58.20±0.10	58.05±0.10	$57.45^{+0.15}_{-0.20}$
146				$60.75^{+0.30}_{-0.50}$
147	60.35±0.10	60.33±0.03	60.78±0.07	60.75±0.10
149	$60.85^{+0.40}_{-0.35}$	61.40±0.10	61.71±0.10	$61.75^{+0.10}_{-0.05}$
150		>61.20−0.15		
151				62.35±0.30
152		<62.40+0.35		
153			62.80±0.05	
155	63.00±0.30	63.90±0.10	63.90±0.10	$64.35^{+0.35}_{-0.30}$
156	63.60±0.05		64.17±0.12	$64.25^{+0.15}_{-0.20}$
160			66.00±0.10	66.25±0.10
166		<68.30+0.05		$68.65^{+0.35}_{-0.15}$
167	$67.95^{+0.15}_{-0.10}$			
169				$69.30^{+0.45}_{-0.40}$

Since the maximum angular momentum brought in by the 110-MeV ^{12}C is close to $\ell_{B_f} = 60\hbar$, the fusion fission mass distribution for 130- or 140-MeV fission will be well approximated with that for 110 MeV when the height is slightly adjusted as depicted with a chain line (A) in Fig. 4 or 5. Hence, the difference (D) between the trapezoidal distribution and A-component is expected to give the fast fission mass distribution. The resulting fast fission mass distribution is consistent with the result obtained for the charge dispersion width (Fig. 2).

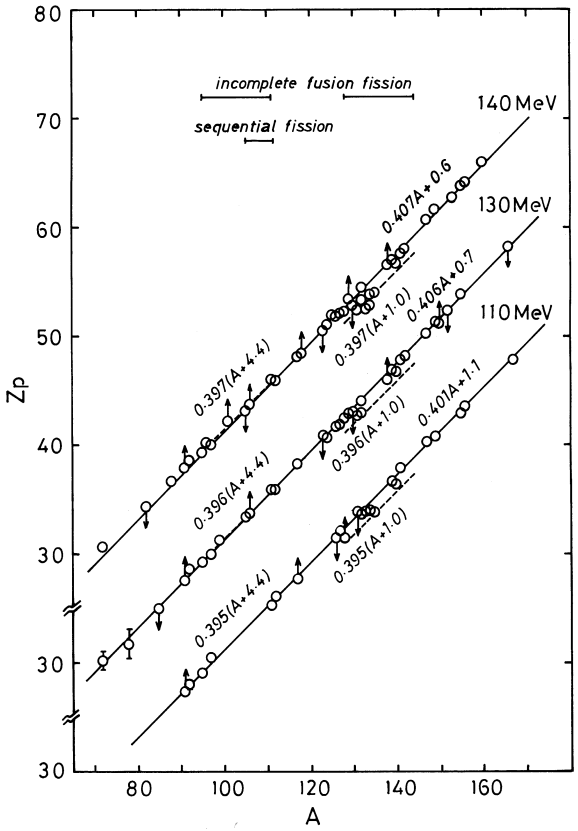

Fig. 3. Determined most probable charges plotted versus mass number. Sold lines represent the charge distribution of complete fusion/fast fission while dashed lines give that of incomplete fusion fission. Horizontal segments of lines indicate the mass regions where the incomplete fusion fission and sequential fission give substantial influence to the mass distribution in the case of the 240-MeV incident energy [23]

The extracted D-component is expressed as

$$\sigma_i(A) = P\exp\{-\frac{(A - A_{i0})^2}{W}\}, \quad i = 1, 2 \qquad (3)$$

and the quantities appearing in (3) are summarized in Table 3 together with the yield ratio of fast fission to complete fusion fission (σ_{fa}/σ_{fu}).

Table 3. Parameters fitted to the Gaussian distributions for fast fission

	FWHM	A_{10}	A_{20}	P	σ_{fa}/σ_{fu}
130 MeV	18.0±0.5	96.5±0.5	148.0±0.5	6±1	0.12
140 MeV	18.0±0.5	96.0±0.5	148.0±0.5	6±1	0.12

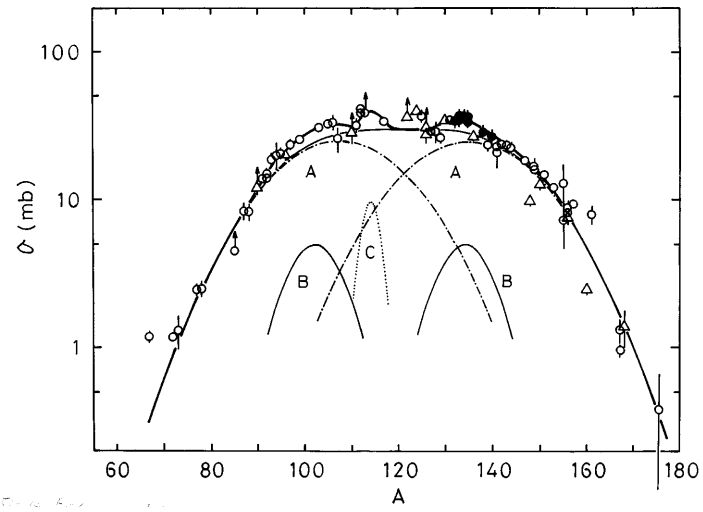

Fig. 4. Mass yield distribution for the 110-MeV ^{12}C beam. Circles represent the total chain yields determined with cumulative yields and triangles designate those obtained from independent yields. Solid marks are the chain yields evaluated by means of the duplicated charge distributions for complete and incomplete fusion fissions. The complete fusion fission component was fitted to a pair of Gaussian distributions represented with chain curves, while a pair of solid Gaussian curves give the incomplete fusion fission. A dotted curve corresponds to the sequential fission by Lee *et al.* [23]

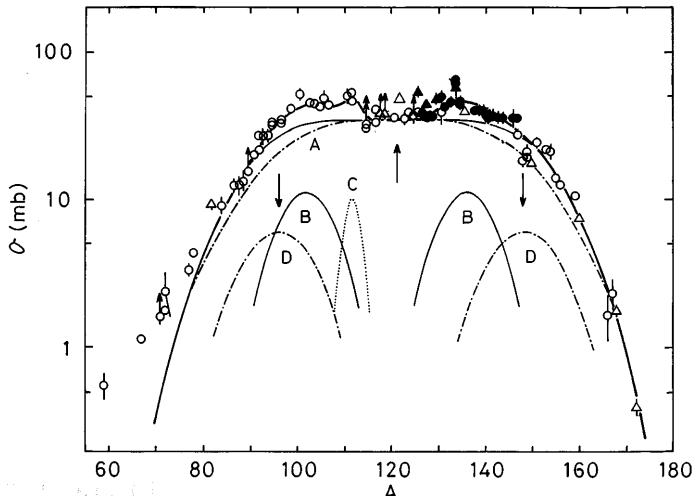

Fig. 5. Mass-yield distribution for the 130-MeV ^{12}C beam. The mass distribution depicted with a solid trapezoidal curve is considered to consist of complete fusion fission and fast fission which is decomposed into complete fusion (a trapezoidal chain curve) and incomplete fusion (a pair of Gaussian chain curves) fissions. The rest are the same as Fig. 4

4 Discussion

The widths of the obtained mass distributions are plotted versus center-of-mass energy $E_{\rm CM}$ in Fig. 6. The widths obtained at lower energies [19] are also added in the figure. The solid circle at 228 MeV is the re-evaluated width for the 240-MeV ^{12}C data [23] using a trapezoidal distribution

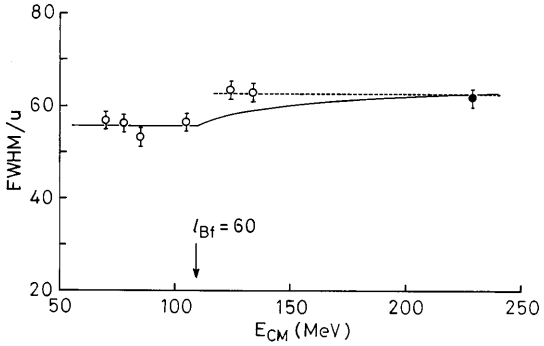

Fig. 6. FWHM of the mass-yield distribution of the complete-fusion/fast fission component as a function of the center-of-mass energy. The solid curve represents the energy dependence of FWHM when it is analyzed as [13]

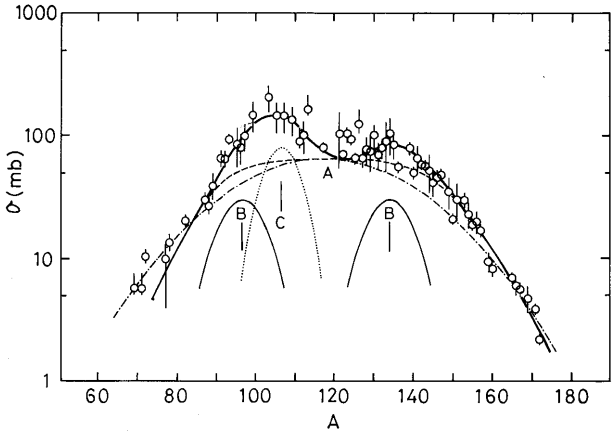

Fig. 7. The mass-yield distribution for the 240-MeV ^{12}C beam [23] in which a trapezoidal curve (dashed line) seems to give a much better fit rather than the Gaussian curve (chain line)

which turns out to reproduce the observed yield data much better than the single Gaussian curve for fusion-plus-fast fission component as depicted in Fig. 7.

Now, let us assume the FWHM of the mass distribution of either of fusion fission or fast fission is constant with respect to the incident energy and angular momentum. Then the total variance σ^2 is expressed in terms of the variances σ_1^2 and σ_2^2 of fusion fission and fast fission, respectively, as [13]

$$\sigma^2 = \begin{cases} \sigma_1^2 & \text{for} \quad \ell_{\max} \le \ell_{B_{\rm f}} \\ \frac{\sigma_1^2(\ell_{B_{\rm f}}+1)^2+\sigma_2^2\{(\ell_{\max}+1)^2-(\ell_{B_{\rm f}}+1)^2\}}{(\ell_{\max}+1)^2} & \text{for} \quad \ell_{\max} > \ell_{B_{\rm f}} \end{cases} \tag{4}$$

with $\ell_{B_{\rm f}} = 60\hbar$ for the (^{238}U + ^{12}C) system [3]. When we assume $\sigma_1^2 = 560$ and $\sigma_2^2 = 762$ (amu)^2 so as to reproduce the FWHM = 65.0 amu at $E_{\rm CM} = 228$ MeV, (4) gives the total width as illustrated with a solid line in Fig. 6.

Observed variances do not, however, follow (4) above the critical energy. Therefore, it is obvious that the width of fast fission can not be controlled by the stiffness coefficient and the temperature as discussed by Grègoire *et al.* [6] but it is rather provoked by the appearance of far-asymmetric mass distribution associated with the set-in

of fast fission as concluded in Figs. 4 and 5. It follows that the mechanism of fast fission is different from that discussed ever.

An alternative reaction mechanism of fast fission one can think of is then the mass drift in the initial trapped system by the diffusion process. One dimensional Fokker-Planck equation [27] is described as

$$\frac{\partial P(x,t)}{\partial t} = \frac{\partial v(x)P(x,t)}{\partial x} + \frac{\partial^2 D(x)P(x,t)}{\partial x^2}, \qquad (5)$$

where $P(x,t)$ is the probability for the system possessing the value x for a given characteristic variable at time t. In the present case where x is the mass number of the product nucleus, D and v are diffusion coefficient and the drift velocity, respectively, which are angular-momentum dependent. They are given for the mass diffusion process [28-32] as

$$D(A_1) = 0.464 \left(\frac{E^*_\ell}{A_c}\right)^{1/4} \left(\frac{A_1^{1/3}A_2^{1/3}}{A_1^{1/3}+A_2^{1/3}}\right)^2 \qquad (6)$$

$$(\text{in} \quad 10^{22}\text{s}^{-1})$$

and

$$v(A_1) = -\frac{D(A_1)}{T_\ell}\frac{\partial U_\ell(A_1,A_2)}{\partial A_1} \qquad (7)$$

with the nuclear temperature

$$T_\ell = 3.46 \left(\frac{E^*_\ell(A_1,A_2)}{A_c}\right)^{1/2}. \qquad (8)$$

E^*_ℓ and U_ℓ are the excitation energy and the driving potential which are given [28] by

$$E^*_\ell = E^*_0 - \frac{e^2}{R_0}\left(\frac{Z_c}{A_c}\right)^2 A_1A_2 - V_p(A_1,A_2) - \frac{\ell(\ell+1)\hbar^2}{2J_{tot}} \qquad (9)$$

and

$$U_\ell(A_1,A_2) = U_{LD}(A_1) + U_{LD}(A_2) - U_{LD}(A_c) + E^*_0 - E^*_\ell(A_1,A_2), \qquad (10)$$

where E^*_0 is the excitation energy for $\ell = 0$ and J_{tot} is the rigid body moment of inertia with the sticking condition

$$J_{tot} = \mu R_0^2 + \frac{2}{5}A_1R_1^2 + \frac{2}{5}A_2R_2^2 \qquad (11)$$

with the reduced mass μ, and the nuclear radii $R_i = r_0A_i^{1/3}(i = 1,2)$ and $R_0 = R_1 + R_2 + d$. Here, we evaluated E^*_ℓ for $\ell = \ell_{B_f}$ since we are dealing with the system just above the critical energy. Furthermore, U_{LD} is the liquid drop energy [33].

V_p is the nuclear attractive potential calculated with the proximity potential $\phi(\xi)$ [34];

$$V_p = 4\pi\gamma R \cdot b\phi(\xi), \qquad (12)$$

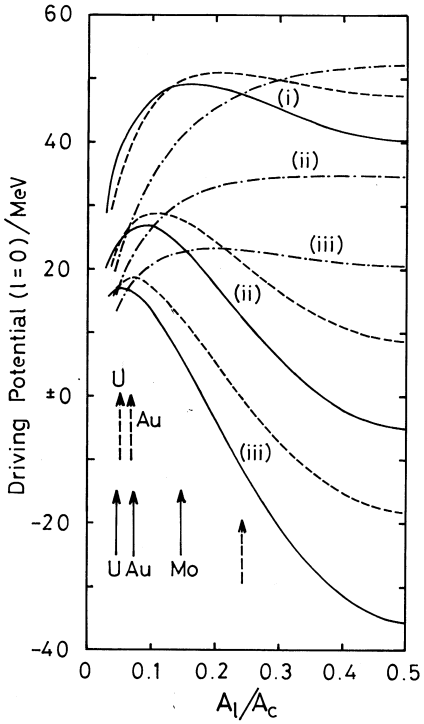

Fig. 8. The driving potential [28] for the $^{12}C + ^{238}U$ (solid curves), $^{16}O + ^{197}Au$ (dashed curves), and $^{16}O + ^{92}Mo$ (dot-dashed curves), calculated with three sets of nuclear radii; (i) $R_0 = R_1+R_2$ and $R_i = 1.2A_i^{1/3}$ fm, (ii) $R_0 = R_1+R_2$ + 0.5 fm and $R_i = 1.36A_i^{1/3}$ fm, and (iii) $R_0 = R_1+R_2$ + 4 fm and $R_i = 1.225A_i^{1/3}$ fm. Solid vertical arrows represent the entrance channels, while dashed vertical arrows give the Businaro-Gallone points of the respective reaction systems

where

$$\gamma = 0.9517[1 - 1.7826(1-2\alpha)^2] \qquad (\alpha = Z_c/A_c) \qquad (13)$$

and

$$R \cdot b \approx \frac{R_1R_2}{R_1+R_2}. \qquad (14)$$

E^*_ℓ and U_ℓ are significantly affected by the nuclear radii, and consequently D and v depend on the radii (particularly on R_0) through E^*_ℓ and U_ℓ. We demonstrate the driving potential U_ℓ ($\ell = 0$) in Fig. 8 for these cases of the nuclear radii; (i) $r_0 = 1.2$ fm and $d = 0$ [28], (ii) $r_0 = 1.36$ fm and $d = 0.5$ fm [30], and (iii) $r_0 = 1.225$ fm and $d = 4$ fm [35]. It is noticed the turning point of the mass drift from symmetric to asymmetric direction shifts toward more asymmetric side as R_0 increases. That is, the influence of R_0 is predominant in determining the direction of mass drift, indifferent of the change in r_0.

If the presently observed fast fission is governed by the diffusion mechanism, we must have the potential driving the entrance channel toward symmetry so that R_0 should take at least the longest among the above three choices. On the other hand, it is well known that the deep-inelastic projectile-like products distribute among elements with smaller Z in such highly mass-asymmetric entrance chan-

Table 4. Computed diffusion coefficient and drift velocity, and the deduced reaction time when E^*_ℓ was assumed to be 33 MeV

D (s^{-1})	$2\sigma^2_A$ (amu^2)	τ (s)	v (s^{-1})	ΔA (amu)	τ (s)
7.8×10^{21}	117	3.7×10^{-21}	2.0×10^{22}	84.5	4.2×10^{-21}

nels [35,36]. Hence, we must construct the driving potential supporting the mass drift in the opposite direction. It follows that the dinuclear system should be more compact in the deep-inelastic collision. Therefore, we conclude from Fig. 8 that the R_0 value of the deep-inelastic collision must not be longer than the case (ii). Bass [37] gives $R_0 = 1.12(A_1^{1/3}+A_2^{1/3})-0.94(A_1^{-1/3}+A_2^{-1/3})+3$ fm with $r_0 = 1.2$ fm, which well reproduces the elastic collision cross sections. Actually, this value of R_0 results in nearly the same driving potential with the case (ii). Therefore, it is very likely that R_0 for the deep-inelastic collision is close to the case (ii). Then fast fission and deep-inelastic collision are different diffusion processes with each other.

The duality of the diffusion process may be interpreted by introducing deformation into the constituents of the dinuclear system. That is, the ordinary deep-inelastic scattering proceeds with the dinuclear configuration consisting of a pair of nearly spherical constituents, while a trapped dinuclear system with high angular momentum eventually develops deformation of one or both of the constituents which results in lowering of the Coulomb interaction by elongation of R_0 or deformation [39].

Though D and v are functions of mass number also, their mass dependence turned out so weak that we can approximately treat them constant in (5). Then, the solution of the Fokker-Planck equation becomes a closed form:

$$P(A,\tau) = (4\pi D\tau)^{-1/2}\exp\left\{-\frac{(A-v\tau)^2}{4D\tau}\right\}. \qquad (15)$$

We can deduce then the life-time τ of fast fission from the observed dispersion and position of the mass distribution as shown in Figs. 4 and 5.

The difference between the initial and final masses in the target-like fragment was found larger than that in the projectile-like fragment by 5.5 mass units as seen in Fig. 4 or 5. This disagreement is interpreted as the prefission neutron emission from the heavy constituent. The average energy required for evaporation of a prefission neutron is known to be 8.0±0.5 MeV for light-particle-induced fission [40,41], and 10±2 MeV for heavy-ion fission [42]. Emission of 5 neutrons, therefore, requires about 50 MeV. In the case of 130-MeV ^{12}C beam, E^*_ℓ is evaluated by (9) to be 58.2 MeV for the case (iii) if no neutrons are emitted during the process. It follows that the average excitation energy of the dinuclear system in the diffusion process may be 33 MeV if neutron emission takes place meanwhile.

Table 4 summarizes the evaluated values of the diffusion coefficient and drift velocity and the resulting life time deduced from the dispersion and position of the mass distribution attributed to fast fission with $E^*_\ell = 33$ MeV. The obtained life times agree with each other and are compared with those of the deep-inelastic reactions determined from

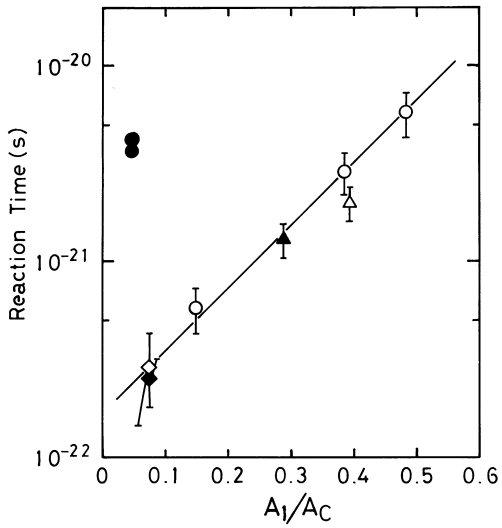

Fig. 9. Reaction times deduced in the present work (solid circles) in comparison with those determined from the angular distributions of projectile-like products; open circles [35], square [36], closed triangles [43], and open triangles [44]

the projectile-like fragment angular distributions [35,36, 43,44] in Fig. 9. The life-times of deep-inelastic scatterings are found linearly depending on the mass-asymmetry with respect to projectiles [35]. On the other hand, the life time of fast fission is more than one order of magnitude longer than the corresponding life time of the deep-inelastic scattering.

Thus, we conclude that the mass relaxation by diffusion is the mechanism of fast fission. The obtained relaxation time is much longer than the life time of deep inelastic scattering but significantly short compared to the fusion fission life time of the order of 3 to 5×10^{-20}s [45-49]. This is consistent with the picture of fast fission being incomplete mass relaxation process as pointed out by Heusch *et al.* [14]. The specification of fast fission being a sort of delayed deep-inelastic process by Nĝo *et al.* [11] also qualitatively agrees with the present conclusion.

The relationship among various types of reaction mechanisms are schematically summarized in Fig. 10, in which the hierarchy of reactions are shown in order of the impact parameters. In the deep-inelastic collision, mass diffusion starts from the initially formed dinuclear system, whereas the once-formed dinuclear system evolves toward a more elongated configuration, likely by deformation of the heavy constituent, and then the mass diffusion takes place in the fast fission. Meanwhile, neutrons are evaporated from the heavy constituent. The mass relaxation in the latter system is eventually interruped at an incomplete stage by the reseparation of the composite system.

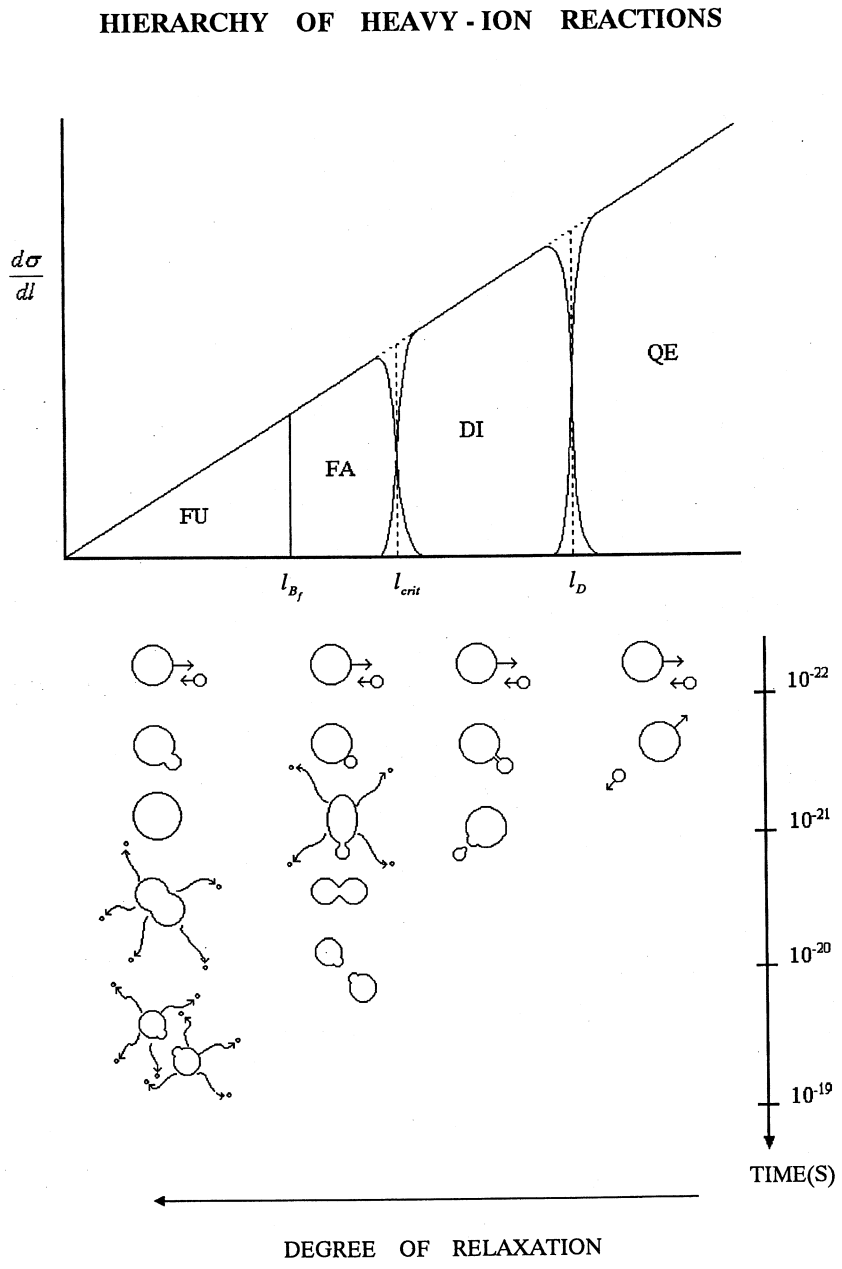

Fig. 10. Schematic illustration of the hierarchy of the reaction mechanism with repect to the angular momentum. The symbols, FU, FA, DI, and QE, stand for fusion fission, fast fission, deep inelastic collision, and quasi-elastic collision, respectively

5 Summary

The reaction of ^{238}U with ^{12}C was studied radiochemically with the purpose of elucidation of fast fission characteristics. From the difference in the mass distribution below and above the critical energy where fast fission is predicted to set in, fast fission component was extracted as a pair of Gaussian distributions in far-asymmetric mass regions. Anomalous charge dispersion widths in the corresponding mass region and a sudden increase of the whole mass distribution width at the critical energy also supported the above result.

Characteristics of the obtained fast fission mass distribution suggested the fast fission mechanism should be governed by the mass diffusion process and were attempted to interpret following the Fokker-Planck equation. The width and position of the Gaussian distribution were analyzed in terms of the computed diffusion coefficient and drift velocity. The resulting life times from the two sources of information agreed with each other to be 4×10^{-21}s when the effective excitation energy was assumed to be 33 MeV considering the effect of neutron emission during the process. The life time turned out to be more than one order of magnitude longer than the corresponding life time of deep inelastic scattering but substantially short compared to ordinary fusion-fission life time.

Evaluation of the driving potential for mass drift required the dinuclear configuration be of a compact form for the deep-inelastic process whereas it should be elongated or deformed for fast fission process. Hence, the dif-

fusion process in fast fission is understood to be different from that of the deep inelastic scattering.

The authors are grateful to Dr. S. Morinobu of Kyushu University for his assistance in operation of the pneumatic irradiation system attached to I course of RCNP. They are also indebted to H. Kobayashi and T. Miyauchi of Osaka University for remodeling and maintenance of the irradiation system.

References

1. Cohen, S., Plasil, F., Swiatecki, W. J.: Ann. Phys. (N.Y.) **82**, 557 (1974)
2. Mustafa, M. G., Baisden, P. A., Chandra, H.: Phys. Rev. **C25**, 2524 (1982)
3. Sierk, A. J.: Phys. Rev. **C33**, 2039 (1986)
4. Baba, H., Shinohara, A., Saito, T., Takahashi, N., Yokoyama, A., J. Phys. Soc. Jpn. **66**, 998 (1997)
5. Lebrun C., Hanappe, F., Lecolley, J. F., Lefebvres, F., Ngô, C., Péter, J., Tamain, B.: Nucl. Phys. **A321**, 207 (1979)
6. Grégoire, C., Lucas, R., Ngô, C., Schürmann, B., Ngô, H.: Nucl. Phys. **A361**, 443 (1981)
7. Borderie, B., Berlanger, M., Gardès, D., Hanappe, F., Nowicki, L., Péter, J., Tamain, B.: Z. Phys. A **299**, 263 (1981)
8. Grégoire, C., Ngô, C., Remaud, B.: Nucl. Phys. **A383**, 392 (1982)
9. Grégoire, C., Ngô, C., Tomasi, E., Remaud, B., Scheuter, F.: Nucl. Phys. **A387**, 37c (1982)
10. Hefter, E. F.: Il Nuovo Cimento **72A**, 1 (1982)
11. Ngô, C., Grégoire, C., Remaud, B., Tomasi, E.: Nucl. Phys. **A400**, 259c (1983)
12. Zheng, Z., Borderie, B., Gardes, D., Gauvin, H., Hanappe, F., Peter, J., Rivet, M. F., Tamain, B., Zaric, A.: Nucl. Phys. **A422**, 447 (1984)
13. Leray, S., Chen, X. S., Fan, G. Y., Grégoire, C., Ho, H., Mazur, C., Ngô, C., Pfoh, A., Ribrag, M., Schad, L., Tomasi, E., Wurm, J. P.: Nucl. Phys. **A423**, 175 (1984)
14. Heusch, B., Freiesleben, H., Schneider, W. F. W., Kohlmeyer, B., Stege, H., Pühlhofer, F.: Z. Phys. A **322**, 309 (1985)
15. Van Geertruyden, A., Leclercq-Willain, Ch.: Nucl. Phys. **A459**, 173 (1986)
16. Van Geertruyden, A., Leclercq-Willain, Ch.: Nucl. Phys. **A459**, 196 (1986)
17. Gippner, P., Brosa, U., Feldmeier, H., Schmidt, R.: Phys. Lett. B **252**, 198 (1990)
18. Takahashi, N., Yukawa, N., Kobayashi, H., Yokoyama, A., Saito, T., Baba, H.: Z. Phys. A **353**, 35 (1995)
19. Duh, M.-C., Baba, H., Takahashi, N., Yokoyama, A., Saito, T., Baba, S., Hata, K.: Nucl. Phys. **A550**, 281 (1992)
20. Baba, H., Okashita, H., Baba, S., Suzuki, T., Umezawa, H., Natsume, H.: J. Nucl. Sci. Tech. (Tokyo) **8**, 703 (1971): Baba, H., Sekine, T., Baba, S., Okashita, H.: Japan Atomic Energy Research Institute report, JAERI 1227 (1972)
21. Shirasu, N., Baba, H.: to be published in Japan Atomic Energy Research Institute M-report.
22. Reus, U., Westmeier, W.: At. Data and Nucl. Data Tables **29**, 1 (1983): evaluated nuclear structure data file of National Nuclear Data Center, BNL, U.S.A.
23. Lee, C. H., Yu, Y. W., Lee, D., Kudo, H., Moody, K. J., Seaborg, G. T.: Phys. Rev. **C38**, 1757 (1988)
24. Umezawa, H., Baba, S., Baba, H.: Nucl. Phys. **A160**, 65 (1971)
25. Yokoyama, A., Takahashi, N., Nitani, N., Baba, H., Kasuga, R., Yamaguchi, T., Yano, D., Takamiya, K., Shinohara, N., Tsukada, K., Hatsukawa, Y., Nagame, Y.: Z. Phys. A **356**, 55 (1996)
26. Baba, H., Yokoyama, A., Takahashi, N., Nitani, N., Kasuga, R., Yamaguchi, T., Yano, D., Takamiya, K., Shinohara, N., Tsukada, K., Hatsukawa, Y., Nagame, Y.: Z. Phys. A **356**, 61 (1996)
27. Nörenberg, W.: Phys. Lett. **53B**, 289 (1974)
28. Wolschin, G., Nörenberg, W.: Z. Phys. A **284**, 209 (1978)
29. Riedel, C., Wolschin, G., Nörenberg, W.: Z. Phys. A **290**, 47 (1979)
30. Ayik, S., Schürmann, B., Nörenberg, W.: Z. Phys. A **279**, 145 (1976)
31. Ayik, S., Schürmann, B., Nörenberg, W.: Z. Phys. A **277**, 299 (1976)
32. Schmidt, R., Toneev, V. D., Wolschin, G.: Nucl. Phys. **A311**, 247 (1978)
33. Myers, W. D., Swiatecki, W. J.: Nucl. Phys. **A81**, 1 (1966)
34. Blocki, J., Randrup, J., Swiatecki, W. J., Tsang, C. F.: Ann. Phys. (N.Y.) **105**, 427 (1977)
35. Agarwal, S.: Z. Phys. A **297**, 41 (1980)
36. Yokoyama, A., Saito, T., Baba, H., Hata, K., Nagame, Y., Ichikawa, S., Baba, S., Shinohara, A., Imanishi, N.: Z. Phys. A **332**, 71 (1989)
37. Bass, R.: "Nuclear Reactions with Heavy Ions", Springer-Verlag, Berlin Heidelberg New York, p.403 (1980)
38. Abe, M.: KEK Report No. 86-26, KEK TH-28 (1986)
39. Quentin, P. P.: J. Phys. (Paris) **30**, 497 (1969)
40. Leachman, R. B.: Proc. Second Int. Conf. on the Peaceful Uses of Atomic Energy, Geneva, Paper P/2467 (1958)
41. Bondarenko, I. I., Kuzminov, B. D., Kutsayeva, L. S., Prokhorova, L. I., Smirenkin, G. N.: Proc. Second Int. Conf. on the Peaceful Uses of Atomic Energy, Geneva, Paper P/2187 (1958)
42. Newton, J. O., Hinde, D. J., Charity, R. J., Leigh, J. R., Bokhorst, J. J. M., Chatterjee, A., Foote, G. S., Ogaza, S.: Nucl. Phys. **A483**, 126 (1988)
43. Wolf, K. L., Unik, J. P., Huizenga, J. R., Birkelund, J., Freiesleben, H., Viola, V. E.: Phys. Rev. Lett. **33**, 1105 (1974)
44. Schröder, W. U., Birkelund, J. R., Huizenga, J. R., Wolf, K. L., Unik, J. P., Viola. Jr., V. E.: Phys. Rev. Lett. **36**, 514 (1976)
45. Hinde, D. J., Ogata, H., Tanaka, M., Shimoda, T., Takahashi, N., Shinohara, A., Wakamatsu, S., Katori, K., Okamura, H.: Phys. Rev. **C39**, 2268 (1989)
46. Hinde, D. J., Hilscher, D., Rossner, H.: Nucl. Phys. **A502**, 497c (1989)
47. Lestone, J. P., Leigh, J. R., Newton, J. O., Hinde, D. J., Wei, J. X., Chen, J. X., Elfstrom, S., Popescu, D. G.: Phys. Rev. Lett. **67**, 1078 (1991)
48. Hofman, D. J., Back, B. B., Diószegi, I., Montoya, C. P., Schadmand, S., Varma, R., Paul, P.: Phys. Rev. Lett. **72**, 470 (1994)
49. Saxena, A., Chatterjee, A., Choudhury, R. X., Kapoor, S. S., Nadkarni, D. M.: Phys. Rev. **C49**, 932 (1994)